Pramana – J. Phys. (2019) 93:102
https://doi.org/10.1007/s12043-019-1865-5

Vibrational resonance in a higher-order nonlinear damped oscillator with rough potential

J A LAOYE[1], T O ROY-LAYINDE[1,2], K A OMOTESO[1], O O POPOOLA[1] and U E VINCENT[3,4,*]

[1]Department of Physics, Olabisi Onabanjo University, Ago-Iwoye, Nigeria
[2]Department of Physics, University of Ibadan, Ibadan, Nigeria
[3]Department of Physical Sciences, Redeemer's University, Ede, Osun State, Nigeria
[4]Department of Physics, Lancaster University, Lancaster LA1 4YB, UK
*Corresponding author. E-mail: u.vincent@lancaster.ac.uk

MS received 20 March 2019; revised 30 July 2019; accepted 21 August 2019

Abstract. We examine the vibrational resonance (VR) of particles moving in a strongly nonlinear damped medium with a harmonically perturbed potential consisting of a background smooth triple-well potential superimposed by a fast oscillating periodic function and subjected to weak and high-frequency (HF) driving forces. The combined effects of the nonlinear damping inhomogeneity and roughness induced by the harmonic perturbation on the phenomenon of VR were theoretically and numerically analysed. It was found that damping inhomogeneity contributed significantly to the enhancement of resonant states, while potential roughness can be optimised by the HF signal to assist resonance enhancement. Furthermore, the traditional smooth VR shapes occurring in the absence of roughness experienced significant distortion occasioned by potential roughness manifesting as spikes that could ultimately be optimised by large amplitudes of the fast signal to energetically facilitate the potential barrier crossing process, thereby enabling VR enhancement.

Keywords. Oscillations; vibrations; fluctuations; resonance; nonlinear dissipation.

PACS Nos 12.60.Jv; 12.10.Dm; 98.80.Cq; 11.30.Hv

1. Introduction

The phenomenon of vibrational resonance (VR) [1] has attracted a lot of attention due to its various applications in weak signal detection [2,3], signal output filtering and attenuation of unwanted signal that are highly applicable in the field of communication, particularly in signal transmissions on different frequencies. The phenomenon is closely related to the already well-studied stochastic resonance [4,5] and other forms of nonlinear resonances which do not directly imply frequency matching such as chaotic resonance [6], coherence resonance [7], parametric resonance [8], ghost resonance [9], autoresonance [8] and antiresonance [10]. VR employs the cooperation between two input signals with significantly varying frequencies – a weak low-frequency (LF) signal and a fast high-frequency (HF) signal – to improve the quality of output of the weak LF signal. Theoretical studies (see, among the others, [11–20]) on VR have been realised in physical experiments (see, among the others, [21–23]).

At resonance, bifurcation of effective potential of slow motion of the system takes place and for this reason, attention of researchers has been drawn to the possible complementary roles played by the system's innate bifurcation parameters [24–26], delay terms [27–29], fractional-order terms [30,31], nonlinear dissipation terms [32–34] and potential deformation [35] on the induction and control of VR. More recently, it was shown that system parameters can be adjusted to control the depth and location of wells in the system potential to optimise VR [36] in a quintic oscillator. VR has been studied in several systems, including the linearly damped quintic oscillators with detailed examination of the contributions of the parameters of the driving signals [37,38] as well as the role of fractional-order coefficients to the effective potential [39].

Despite the stimulating and several intriguing realisations and observations of VR in many systems (see refs [13,14,16,17,26–30,37,39–42]), we emphasise that all these examples relate to systems whose potentials

Published online: 15 October 2019

are assumed to be smooth. In practice, however, the potentials that are encountered frequently when studying the stability of stationary solutions for several important physical, engineering and biophysical problems are usually nonsmooth, but characterised by spatial impurities or inhomogeneities that can lead to deviations from smooth surfaces evidenced by potential roughness [43–45]. Indeed, from the biophysical perspective, potential roughness carries significant implication in protein folding manifested by rich hierarchial structure and may better describe also the dynamics of any physical system which may not be precisely captured with smooth potential representation [46,47]. Roughness in potential landscape is measurable and has been experimentally realised in, for instance, proteins folding [48,49] and compacted graphite iron [50,51]. Studies have shown that the presence of roughness could lead to quite different transport properties in comparison with the smooth case and can specifically enhance [52] or in some cases, hinder/counter significantly directed transport or eliminate it totally [53–55]. Roughness may also alter system dynamics or induce physical phenomena such as chaos, current reversal, anomalous diffusion [48] as well as speeding up the process of barrier crossing [56]. These interesting results which raise naturally, the question on the possible constructive and/or destructive role of roughness in the occurrence of VR constitute our main motivations for considering the effect of rough potential function on VR.

In general, the system's potential $V(x)$ may consist of a smooth background $V_0(x)$ superimposed by a rapidly and randomly-varying space-dependent harmonic perturbation $V_1(x)$, such that $V(x) = V_0(x) + V_1(x)$. It can simply be interpreted as the potential surface of a system with hierarchical structure, with small potential well embedded in large potential well (a description is presented by Zwanzig [46]).

In this paper, we investigate, for the first time, the VR of a periodically-driven particle moving in a strongly nonlinear damped medium with a harmonically perturbed potential consisting of a background smooth triple-well potential superimposed by a fast oscillating periodic function, and subjected to a second HF driving forces. We focus our attention on the effects of nonlinearity in the damping term and the perturbation-induced roughness on the system's response to HF signal. We assume mild fluctuations on the smooth potential such that no well is sufficiently wide to trap the particle other than the wells from the smooth background. Our assumption is in contrast with the one expressed in [57] where small fluctuations on the system potential were considered so that the strength of the harmonic perturbation can be modulated to increase the number of wells, hence optimise the response.

2. The model

The model system considered here is a dimensionless nonlinear oscillator with a triple-well potential and derived from a two-fluid magnetised plasma oscillator constructed from a set of quasihydrodynamic equations of motion given by [58]

$$\frac{\mathrm{d}^2\tilde{n}}{\mathrm{d}\tau^2} - \frac{\mathrm{d}S_i}{\mathrm{d}\tau} + \nu_i\left(S_i - \frac{\mathrm{d}\tilde{n}}{\mathrm{d}\tau}\right) = \frac{in_0k_z}{m_i}\cdot(\tilde{v}\times\widetilde{\vec{B}_0}) - \frac{K_\mathrm{B}k_z^2}{m_i}(T_\mathrm{e}+\gamma T_\mathrm{i})\tilde{n} + \frac{en_0}{m_i}\nabla\cdot\vec{E}_1, \tag{1}$$

where $\tilde{n}$ is related to the ion density, ν_i is the neutral collision frequency, m_i is the specie's (ion) mass, $\vec{E}_1 = E_0\sin(\omega t + k_z z)$ is the externally applied electric field, $\widetilde{\vec{B}_0}$ is the applied magnetic field and $\tilde{v}$ is the ion flow velocity. The quantity n_0 arises from the imposed conditions in which a small amplitude waves for a uniform infinite plasma is assumed. From thermodynamics formalism, the ion source term, S_i, is given by the following expression:

$$S_i = \alpha_1\tilde{n} + \alpha_2\tilde{n}^2 + \alpha_3\tilde{n}^3 + \alpha_4 + \tilde{n}^4 + \alpha_5\tilde{n}^5 + \cdots, \tag{2}$$

where the subscript i stands for ion and α_j ($j\in\{2,3,4,5\}$) are the coefficients which are dependent on the type of ion source in use. Note that if $j = 1$, then, α_1 is a linear coefficient, otherwise ($j \neq 1$), the coefficients are nonlinear. The other quantities T_i and T_e ($T_\mathrm{i} \ll T_\mathrm{e}$) are respectively the ion and electron temperatures, while k_z and K_B are the axial wave number and the Boltzmann's constant, respectively.

Suppose a strong nonlinear interaction is considered. Then, the quadratic terms in S_i are negligible (i.e. $\alpha_2 = \alpha_4 = 0$). By substituting eq. (2) in (1) and considering a slap geometry for which density varies in the x-direction and the z-axis coinciding with the magnetic field direction, then, it is easy to show that the equation for the dynamics is given as [59]

$$\frac{\mathrm{d}^2\tilde{n}}{\mathrm{d}\tau^2} - (\nu_i + \alpha_1 + 3\alpha_3\tilde{n}^2 - 5\alpha_5\tilde{n}^4)\frac{\mathrm{d}\tilde{n}}{\mathrm{d}\tau} + \omega_0^2\tilde{n} + \nu_i\alpha_5\tilde{n}^5 = \tilde{f}\cos(\tilde{\omega}\tau), \tag{3}$$

where

$$\omega_0^2 = \frac{k_z^2K_\mathrm{B}(T_\mathrm{e}+\gamma T_\mathrm{i})}{m_i} + \nu_i\alpha_1.$$

ω_0 is the ion sound instability frequency given as $\omega_0 = k_z C_s$, and

$$C_s = \sqrt{\frac{k_z^2 K_B(T_e + \gamma T_i)}{m_i}}$$

is the ion sound velocity.

In general, $\omega_0^2 \gg \nu_i, \alpha_3\tilde{n}^2$, and $\alpha_5\tilde{n}^4$. In eq. (3), the damping function is dependent on the linear growth ($\nu_i + \alpha_1$) and the nonlinear coefficients (α_3 and α_5). ω_0 is the characteristic angular frequency, α_3 and $\nu_i\alpha_5$ are nonlinear coefficients of restoring force, $\tilde{\omega}$ is the angular frequency of the externally excited wave of amplitude $\tilde{f}$. By setting

$$t = \omega_0\tau, \quad x = \sqrt{-\frac{3\alpha_3}{\alpha_1 + \nu_1}}\tilde{n}, \quad \mu = \frac{\alpha_1 + \nu_i}{\omega_0},$$

$$\gamma = \frac{5\alpha_5(\nu_i + \alpha_1)}{9\alpha_3^2}, \quad \lambda = -\frac{\nu(\alpha_1 + \nu_i)}{3\omega_0^2}, \quad \omega = \frac{\tilde{\omega}}{\omega_0},$$

$$\beta = \frac{\nu_i\alpha_5(\alpha_1 + \nu_i)^2}{9\alpha_3^2\omega_0^2}, \quad f = \frac{n_0 k_z e E_0}{m_i} \tag{4}$$

and dropping the tildes where applicable, the dimensionless equation of motion is obtained as

$$\frac{d^2x}{dt^2} - \mu(1 - x^2 + \gamma x^4)\frac{dx}{dt} + x + \lambda x^3 + \beta x^5 = f\cos(\omega t). \tag{5}$$

Here, we consider the mildly perturbed biharmonically driven form of eq. (5) given as

$$\ddot{x} - \mu(1 - x^2 + \gamma x^4)\dot{x} + \frac{dV}{dx} = f\cos\omega t + g\cos\Omega t, \tag{6}$$

where μ is the damping parameter and γ is the higher-order nonlinear damping coefficient. In our recent papers, we had explored the occurrence of VR and the associated mechanisms in systems with nonlinear damping due to their numerous applications as detailed in [33,34]. The potential $V(x)$ is given by

$$V(x) = V_0(x) + V_1(x),$$

$$V_0(x) = \frac{x^2}{2} + \frac{\lambda x^4}{4} + \frac{\beta x^6}{6},$$

$$V_1(x) = \epsilon(\cos\omega_1 x + \sin\omega_2 x), \tag{7}$$

with ϵ being the amplitude of roughness. For the present study, we have chosen $\epsilon \ll 1$ to imply mild perturbation, $\omega_1 = 167$ and $\omega_2 = 73$ are fixed throughout the paper. Figure 1 shows the smooth potential V_0 for $\lambda = -0.6$ and three different values of β. In this study, we shall consider the triple well potential at $\beta = 0.07$ and $\lambda = -0.6$. Now, for $\epsilon \neq 0$, the perturbed potential surface becomes increasingly rough with increasing ϵ as illustrated in the upper panel (UP) of figures 2a–2d for $\epsilon = 0, 0.05, 0.1$ and 0.3 respectively. The perturbation has a typical length scale, and when $V(x)$ is spatially averaged over Δx, the perturbation is eliminated and only the smooth background remains.

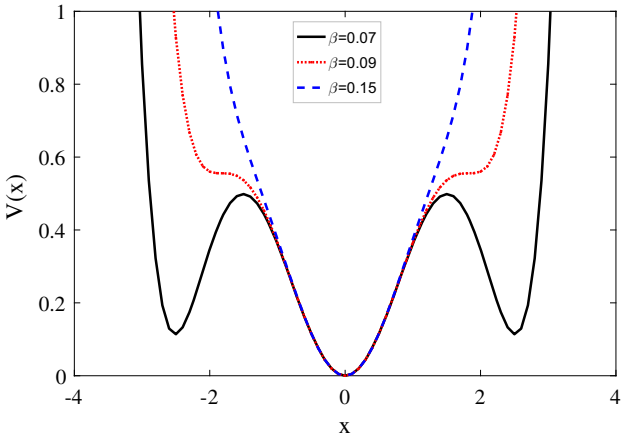

Figure 1. The system's smooth potential (V_0) for three values of β (0.07, 0.09 and 0.15) when $\lambda = -0.6$.

By setting polynomial terms in the nonlinear damping of system (6) to zeroes and ϵ=0, our model system reduces to the exact forms of the quintic oscillator already considered in [36,37] without rugged landscape. The quintic oscillator has received considerable attention due to its numerous applicability in modelling of nonlinear systems. Particularly, plasma oscillation has been modelled as a damped driven quintic oscillator with higher-order nonlinear dissipation [60], while the effects of HF and LF signals on plasma propagation in theory, experiments and direct applications are useful in understanding modern science and technology [61–65]. It is also worth mentioning that in practice, the quantum efficiency, gain and output field squeezing of single-mode Josephson-junction-based parametric amplifier devices can be limited by neglecting the effects of higher-order corrections to the idealised model [66,67]

3. Theoretical analysis

System (6) is driven by periodic forces, $f\cos(\omega t)$ and $g\cos(\Omega t)$, with $\Omega \gg \omega$. So its motion is assumed to consist of a combination of slow motion $\chi(t)$ with frequency ω and of a fast motion $\psi(t, \tau = \Omega t)$ with frequency Ω. We employ the method of direct separation of motions (DSM) to obtain a set of integro-differential equations, one of which is the equation of slow motion of the system whose response can be modulated by varying the

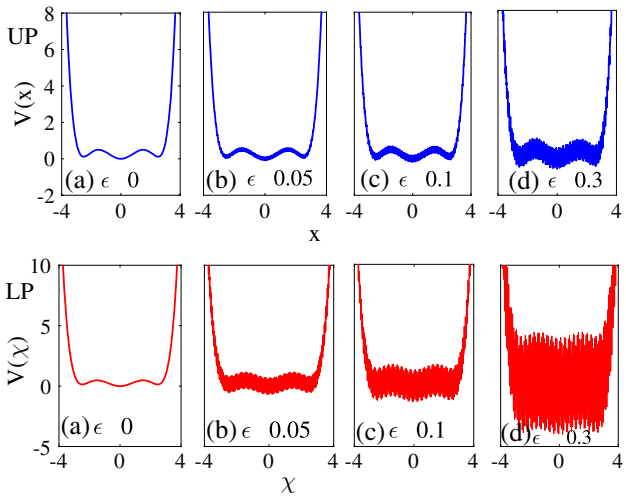

Figure 2. Effect of roughness on the system potential for four values of amplitude ϵ (=0, 0.05, 0.1 and 0.3) is shown in figures a, b, c and d of the upper panel (UP) respectively while the effect of the same values of roughness amplitude on the system's effective potential, computed from eq. (22) is shown in figures a, b, c and d of the lower panel (LP) respectively. Other parameters are: $\beta = 0.07, \lambda = -0.6, \Omega = 5, g = 15$, $\omega_1 = 167$ and $\omega_2 = 73$.

parameters of the HF input drive. By solving the equation for the slow motion, the response amplitude, Q, which provides an idea of how the weak output is modulated by the parameters of the fast signal can be obtained. The fundamental idea of the DSM is to consider the solution $x(t)$ of system (6) as a superposition of only the solutions $\chi(t)$ of slow evolution with frequency ω and $\psi(t)$ of the fast oscillations with frequency $\Omega(t)$ when $\Omega \gg \omega$, in the form:

$$x(t) = \chi(t) + \psi(t, \Omega t), \tag{8}$$

where $\chi(t)$ and $\psi(t)$ are periodic with period $T = 2\pi/\omega$ and $2\pi/\Omega$ respectively. The mean value of the fast signal ψ with respect to fast time $\tau = \Omega t$ is given by

$$\langle\psi\rangle = \frac{1}{2\pi}\int_0^{2\pi} \psi \, \mathrm{d}\tau = 0. \tag{9}$$

The first of the 2-coupled integro-differential equations for the variables χ and ψ is obtained by substituting eq. (8) in eq. (6) to yield

$$\begin{aligned}
&\ddot{\chi} + \ddot{\psi} - \mu[1 - (\chi+\psi)^2 + \gamma(\chi+\psi)^4](\dot{\chi}+\dot{\psi}) \\
&\quad +(\chi+\psi) + \lambda(\chi+\psi)^3 + \beta(\chi+\psi)^5 \\
&\quad +\epsilon\omega_2 \cos\omega_2(\chi+\psi) - \epsilon\omega_1 \sin\omega_1(\chi+\psi) \\
&= f\cos\omega t + g\cos\Omega\tau,
\end{aligned} \tag{10}$$

and then averaging both sides of eq. (10) over the period of fast time $[0, 2\pi/\Omega]$ and applying eq. (9), we then obtain

$$\begin{aligned}
&\ddot{\chi} + \mu[1 - (\chi^2 + \langle\psi^2\rangle) + \gamma(\chi^4 + \langle\psi^4\rangle + 6\chi^2\langle\psi^2\rangle)]\dot{\chi} \\
&\quad +(1 + 3\lambda\langle\psi^2\rangle + 5\beta\langle\psi^4\rangle)\chi \\
&\quad +(\lambda + 10\beta\langle\psi^2\rangle)\chi^3 + \beta\chi^5 \\
&\quad +\epsilon\omega_2\cos\omega_2\chi\langle\cos\omega_2\psi\rangle - \epsilon\omega_2\sin\omega_2\chi\langle\sin\omega_2\psi\rangle \\
&\quad -\epsilon\omega_1\sin\omega_1\chi\langle\cos\omega_1\psi\rangle - \epsilon\omega_1\cos\omega_1\chi\langle\sin\omega_1\psi\rangle \\
&= f\cos\omega t + \langle g\cos\Omega t\rangle.
\end{aligned} \tag{11}$$

By defining the following mean values,

$$\begin{aligned}
&\langle g\cos\Omega t\rangle = 0, \\
&\langle\sin\omega_i\psi\rangle = \frac{1}{2\pi}\int_0^{2\pi}\sin\omega_i\psi \, \mathrm{d}\tau = 0, \quad i = 1, 2 \\
&\langle\cos\omega_i\psi\rangle = \frac{1}{2\pi}\int_0^{2\pi}\cos\omega_i\psi \, \mathrm{d}\tau = J_0(\omega_i\psi_0), \\
&\quad i = 1, 2,
\end{aligned} \tag{12}$$

where $J_0(\psi_0)$ is the zeroth-order Bessel function of the first kind and ψ_0 is a constant, eq. (11) can be further simplified to give

$$\begin{aligned}
&\ddot{\chi} - \mu[1 - (\chi^2 + \langle\psi^2\rangle) \\
&\quad +\gamma(\chi^4 + \langle\psi^4\rangle + 6\chi^2\langle\psi^2\rangle)]\dot{\chi} \\
&\quad +(1 + 3\lambda\langle\psi^2\rangle + 5\beta\langle\psi^4\rangle)\chi + (\lambda + 10\beta\langle\psi^2\rangle)\chi^3 \\
&\quad +\beta\chi^5 + \epsilon\omega_2 J_0(\omega_2\psi_0)\cos\omega_2\chi \\
&\quad -\epsilon\omega_1 J_0(\omega_1\psi_0)\sin\omega_1\chi = f\cos\omega t.
\end{aligned} \tag{13}$$

Equation (13) is the first of the set of coupled equations for the variable χ. The other pair of the set of equations is obtained by subtracting eq. (13) from eq. (10), that is

$$\begin{aligned}
&\ddot{\psi} - \mu[1 - (\chi+\psi)^2 + \gamma(\chi+\psi)^4]\dot{\psi} \\
&-\mu[-2\chi(\psi - \langle\psi\rangle) - \chi(\psi^2 - \langle\psi^2\rangle) \\
&+4\gamma\chi^3(\psi - \langle\psi\rangle) + 6\gamma\chi^2(\psi^2 - \langle\psi^2\rangle) \\
&+4\gamma\chi(\psi^3 - \langle\psi^3\rangle) + \gamma(\psi^4 - \langle\psi^4\rangle)]\dot{\chi} \\
&+\psi + \lambda(\psi^3 - \langle\psi^3\rangle) + 3\lambda\chi(\psi^2 - \langle\psi^2\rangle) \\
&+3\lambda\chi^2(\psi - \langle\psi\rangle) + \beta(\psi^5 - \langle\psi^5\rangle) \\
&+5\beta\chi^4(\psi - \langle\psi\rangle) \\
&+5\beta\chi(\psi^4 - \langle\psi^4\rangle) + 10\beta\chi^3(\psi^2 - \langle\psi^2\rangle) \\
&+10\beta\chi^2(\psi^3 - \langle\psi^3\rangle) + 10\beta\chi^2\langle\psi^3\rangle + R_* \\
&\quad = g\cos\Omega\tau,
\end{aligned} \tag{14}$$

where

$$R_* = \epsilon\omega_2 \cos\omega_2\chi\,(\cos\omega_2\psi - \langle\cos\omega_2\psi\rangle) - \epsilon\omega_2 \sin\omega_2\chi \sin\omega_2\psi - \epsilon\omega_1 \sin\omega_1\chi\,(\cos\omega_1\psi - \langle\cos\omega_1\psi\rangle) + \epsilon\omega_1 \cos\omega_1\chi \sin\omega_1\psi.$$

Equation (14) is then approximated using the inertial approximation $\ddot{\psi} \gg \dot{\psi} \gg \psi$ by considering ψ to be a rapidly oscillating variable whose long-term solution is periodic in fast time in the form

$$\ddot{\psi} - \mu\dot{\psi} = g\cos\Omega t, \tag{15}$$

having the steady-state solution

$$\psi = \psi_0 \cos(\omega t + \theta) = \frac{g}{\Omega\sqrt{\Omega^2 + \mu^2}} \cos(\omega t + \theta), \tag{16}$$

where

$$\sin\theta = \frac{\mu}{\sqrt{\Omega^2 + \mu^2}}, \quad \cos\theta = \frac{-\Omega}{\sqrt{\Omega^2 + \mu^2}} \tag{17}$$

and ψ_0 may be approximated by assuming $\Omega \gg \mu$, so that

$$\psi_0 = \frac{g}{\Omega^2}. \tag{18}$$

Equation (13) can now be written as

$$\ddot{\chi} - \mu(C_1 - C_2\chi^2 + \gamma\chi^4)\dot{\chi} + C_3\chi + C_4\chi^3 + \beta\chi^5 + \epsilon\omega_2 J_0\left(\frac{\omega_2 g}{\Omega^2}\right)\cos\omega_2\chi - \epsilon\omega_1 J_0\left(\frac{\omega_1 g}{\Omega^2}\right)\sin\omega_1\chi = f\cos\omega t, \tag{19}$$

where

$$C_1 = \left(1 - \frac{g^2}{2\Omega^4} + \frac{3\gamma g^4}{8\Omega^8}\right), \quad C_2 = \left(1 - \frac{3\gamma g^2}{\Omega^4}\right),$$
$$C_3 = \left(1 + \frac{3\lambda g^2}{2\Omega^4} + \frac{15\beta g^4}{8\Omega^8}\right),$$
$$C_4 = \left(\lambda + \frac{5\beta g^2}{\Omega^4}\right). \tag{20}$$

Equation (19) is the fast signal parameter-dependent equation of slow oscillation, providing the tools for the weak signal modulation at the lower frequency by parameters of the fast signal. Equation (19) can simply be written as

$$\ddot{\chi} + \alpha_{\text{eff}}\dot{\chi} + \frac{\mathrm{d}V_{\text{eff}}}{\mathrm{d}\chi} = f\cos\omega t, \tag{21}$$

where

$$V_{\text{eff}} = C_3\frac{\chi^2}{2} + C_4\frac{\chi^4}{4} + \beta\frac{\chi^6}{6} + \epsilon J_0\left(\frac{\omega_2 g}{\Omega^2}\right)\sin\omega_2\chi + \epsilon J_0\left(\frac{\omega_1 g}{\Omega^2}\right)\cos\omega_1\chi \tag{22}$$

and

$$\alpha_{\text{eff}} = -\mu(C_1 - C_2\chi^2 + \gamma\chi^4) \tag{23}$$

are the effective potential shown in the lower panel (LP) in figure 2 for four values of roughness amplitude ϵ (= 0, 0.05, 0.1 and 0.3) and the effective dissipation, respectively. In figures 2b–2f of the lower panel, as the roughness amplitude is gradually varied, a series of fine lines showing what could be regarded as many tiny narrow wells which in our analysis are assumed not wide enough to house particles, are shown. It is also visible that, as the system's roughness increases with increase in ϵ, the shape of the potential and the number of well-defined wells from the smooth potential however remain unchanged. In addition, the system's effective potential computed from eq. (22) is presented in figure 3 for six values of amplitude of the fast driving signal, g = 0, 15, 25, 35, 65 and 100 and other parameters, $\beta = 0.07$, $\gamma = 0.6$, $\Omega = 5$, $\omega_1 = 167$, $\omega_2 = 73$ and $\epsilon = 0.02$, are fixed. It is clear that the amplitude g can significantly alter the shape and surface of the potential, with the system making transition from triple well potential (shown in figures 3a–3c) to single well potential in figure 3e–3f, where the perturbation is gradually eliminated leaving behind the smooth background. Notably, this is suggestive of the possibility of large amplitudes of the fast signal being ultimately optimised to energetically facilitate potential barrier crossing process of a particle moving in a rough potential system, thereby enabling VR enhancement as we shall show later. Again, we should emphasise that the effect of system parameters for the case of unperturbed linearly damped system has been thoroughly examined and reported in [36–38].

In the following, we turn to the description of the system's vibrations in terms of the deviation (Y) of the slow motion (χ) from the equilibrium points (χ^*) by substituting the variable Y ($=\chi - \chi^*$) in eq. (19). The equilibrium points around which slow oscillations occur are $\chi^*_{\min(\max)} = 2n\pi$, where n is an integer. Considering the equilibrium points $\chi^* = \chi_{\min(\max)}$, $J_{0_n}\cos n\pi\chi^* = |J_{0_n}|$, $f \ll 1$ and $\cos n\pi Y = 1$, we can discard the higher powers in the deviation Y assuming that $|Y| \ll 1$, so that eq. (19) can then be written as

$$\ddot{Y} - \mu(C_1 - C_2(2Y\chi^* + \chi^{*2}) + \gamma(4Y\chi^{*3} + \chi^{*4}))\dot{Y} + \left(C_3 + 3C_4\chi^{*2} + 5\beta\chi^{*4} + \epsilon\omega_1^2\left|J_0\left(\frac{\omega_1 g}{\Omega^2}\right)\right|\right)Y$$

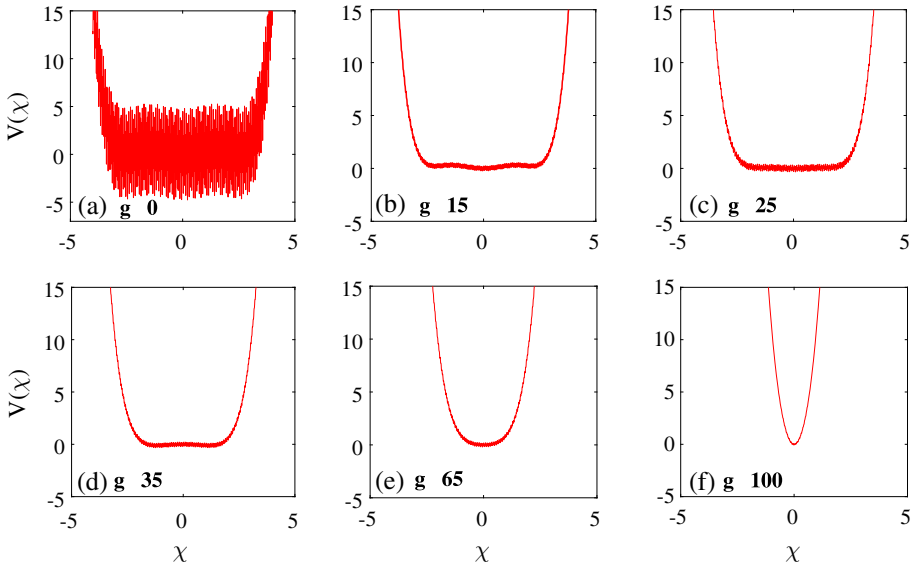

Figure 3. Dependence of the system's effective potential with roughness amplitude $\epsilon = 0.02$ on amplitude of the fast drive $g = 0, 15, 25, 35, 65$ and 100 for figures a, b, c, d, e and f respectively. Other parameters are: $\beta = 0.07$, $\gamma = 0.6$, $\Omega = 5$, $\omega_1 = 167$ and $\omega_2 = 73$.

$$+C_3\chi^* + C_4\chi^{*3} + \beta\chi^{*5}$$
$$+\epsilon\omega_2\left|J_0\left(\frac{\omega_2 g}{\Omega^2}\right)\right| = f\cos\omega t. \tag{24}$$

At the equilibrium points, we can write

$$\ddot{Y} - \mu C_1\dot{Y} + \left(C_3 + \epsilon\omega_1^2\left|J_0\left(\frac{\omega_1 g}{\Omega^2}\right)\right|\right)Y$$
$$+\epsilon\omega_2\left|J_0\left(\frac{\omega_2 g}{\Omega^2}\right)\right| = f\cos\omega t. \tag{25}$$

If we set the damping amplitude as $\alpha = -\mu C_1$ and resonant frequency as

$$\omega_r = \sqrt{C_3 + \epsilon\omega_1^2\left|J_0\left(\frac{\omega_1 g}{\Omega^2}\right)\right|}$$

in eq. (25) we can simply obtain an approximate damped and periodically forced linear equation of the form

$$\ddot{Y} + \alpha\dot{Y} + \omega_r^2 Y = f\cos\omega t, \tag{26}$$

whose steady-state solution describing the ultimate behaviour of the system in the long time limit, $t \to \infty$ is $Y(t) = A_L\cos(\omega t + \Phi)$. Thus, the response amplitude is given as

$$Q = \frac{A_L}{F} = \frac{1}{\sqrt{(\omega_r^2 - \omega^2)^2 + \alpha^2\omega^2}}. \tag{27}$$

In eq. (27), it is clear that Q is maximum when $S = \omega_r^2 - \omega^2$ is minimum, i.e. at resonance, $\omega_r = \omega$. Expectedly the damping inhomogeneity (α) is now a function of the parameters G and Ω of the fast motion while the resonant frequency (ω_r) is dependent on the parameters of roughness, both of which determine the magnitude of Q.

4. Numerical simulations and discussions

In the numerical simulation results that follow, we first expressed eq. (6) as a set of coupled linear autonomous ordinary differential equations of the form

$$\frac{dx}{dt} = y,$$
$$\frac{dy}{dt} = \mu(1 - x^2 + \gamma x^4)y - x - \lambda x^3 - \beta x^5$$
$$-\epsilon(\omega_1\sin\omega_1 x - \omega_2\cos\omega_2 x)$$
$$+f\cos\omega t + g\cos\Omega t \tag{28}$$

and then integrate using the fourth-order Runge–Kutta (RK4) scheme with step size $\Delta t = 0.01T$ over a simulation time interval $T_s = nT$, $T = 2\pi/\omega$ being the period of oscillation where ω is the LF input signal and $n\,(=1, 2, 3, \ldots)$ is the number of complete oscillations. We used initial conditions $(0, 1)$ and a relaxation time of $20T$. Throughout the computation, we fixed system parameter values as $\omega = 0.075$, $f = 0.08$, $\lambda = -0.6$, $\beta = 0.07$ and $\mu = 4$ except otherwise specified. These choices ensure that the system is in the overdamped regime in which only periodic or quasiperiodic motion is admissible. The other system parameters, Ω, γ and g, are chosen within a regime that optimises the emergence of VR. After solving eqs (28) and discarding

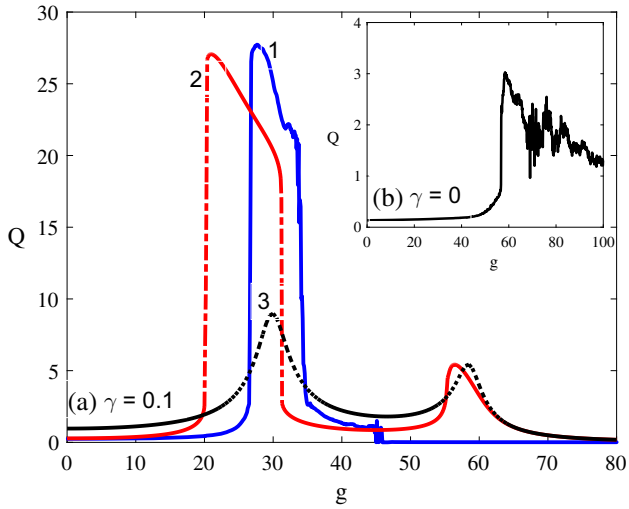

Figure 4. Dependence of the system's response on amplitude of the fast driving force for (**a**) $\gamma = 0.1$ and (**b**) $\gamma = 0$ for unperturbed system ($\epsilon = 0$). Line 1 (continuous line) represents the numerical response curve computed from eq. (28), line 2 (dash–dot line) represents the analytical response curve obtained from eq. (24) and line 3 represents the linearised analytical response curve obtained from eq. (26). Other parameters are: $\lambda = -0.6, \beta = 0.07, \Omega = 5, \omega_1 = 167$ and $\omega_2 = 73$.

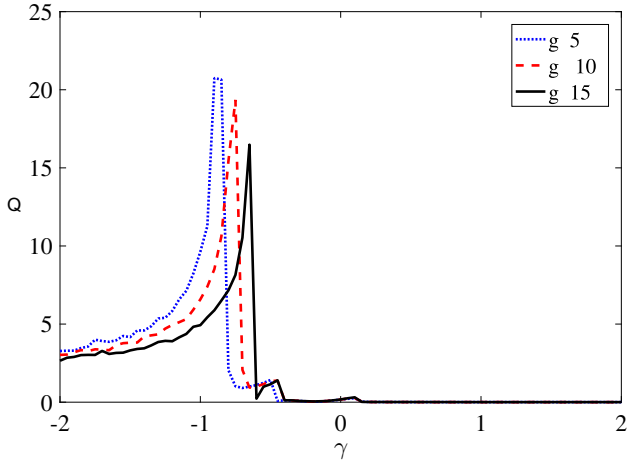

Figure 5. Dependence of the system's response amplitude (Q) on the strength of the higher-order damping inhomogeneity (γ) for three values of amplitude g ($g = 5, 10$ and 15). Other parameters are: $\epsilon = 0, \beta = 0.07, \lambda = -0.6, \omega = 0.075, \Omega = 5, \omega_1 = 167$, $\omega_2 = 73$ and $f = 0.08$.

the transient, the response amplitude (Q) is computed from the expression

$$Q = \frac{\sqrt{Q_s^2 + Q_c^2}}{f}, \tag{29}$$

over a range of values of the HF intensity (g) from the Fourier spectrum of the time series of the output signal (x) with Fourier coefficients Q_s and Q_c, where

$$Q_s = \frac{2}{nT}\int_0^{nT} x(t)\sin\omega t \, \mathrm{d}t$$
$$Q_c = \frac{2}{nT}\int_0^{nT} x(t)\cos\omega t \, \mathrm{d}t \tag{30}$$

and $T = 2\pi/\Omega$ is the period of oscillation of the LF input signal with n (=1, 2, 3, ...) number of complete oscillations. The numerically obtained Q-factors are compared with the corresponding analytical values by superposing the response curves of Q against appropriately chosen parameters for a range of system parameters. The maximum of these curves are the optimal match between the LF and HF that signifies the VR.

We begin by examining the occurrence of VR in the unperturbed system, i.e. $\epsilon = 0$. We fix the following system parameters: $\lambda = -0.6, \beta = 0.07, \Omega = 5, \omega_1 = 167$ and $\omega_2 = 73$. In figure 4 which shows the dependence of the system's response amplitude (Q) on the amplitude of the fast driving force for $\gamma = 0.1$ in figure 4a and $\gamma = 0$ in figure 4b for unperturbed system ($\epsilon = 0$), one can immediately observe the phenomenon of VR on the system with and without higher-order nonlinear inhomogeneity. With Line 1 (continuous line) denoting the numerical response curve obtained from eq. (28), line 2 (dash–dot line) denoting the analytical response curve computed from eq. (24) and line 3 denoting linearised analytical response curve obtained from eq. (26), one can make comparison between analytical results and numerical simulations.

The analytical and the numerical results are qualitatively in agreement, with both displaying similar response shape. However, the response amplitude computed for the linearised system (eq. (26)) shows resonance with lower peak in $Q_{\max}$ compared to the system with higher-order nonlinear damping due to the approximation of higher-order nonlinearity in the damping whose impact is significant on the system's dynamics. For the range of system parameters chosen, the effect of higher-order nonlinear damping on the system response becomes significantly pronounced compared to when $\gamma = 0$ in figure 4b. This is also evident in figure 5 where the response (Q) is plotted against γ, the coefficient of the higher-order nonlinear damping inhomogeneity for three values of amplitude g ($g = 5$, 10 and 15) with other parameters, $\epsilon = 0, \beta = 0.07, \lambda = -0.6$, $\omega = 0.075, \Omega = 5, \omega_1 = 167, \omega_2 = 73$ and $f = 0.08$ fixed. The system is driven into resonant state by increasing the strength of the frictional inhomogeneity as clearly depicted by larger response amplitude obtained for $\gamma < 0$, implying that in situations where large resonant oscillations are desirable, by choosing

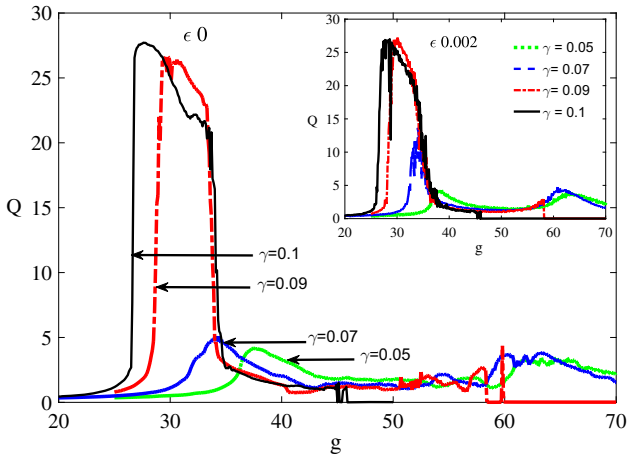

Figure 6. Dependence of Q on the amplitude of the fast drive (g) for four values of strength of the higher-order nonlinear dissipation ($\gamma = 0.05, 0.07, 0.09$ and 0.1) for the system with smooth potential, $\epsilon = 0$. Inset shows the same dependence for rugged potential landscape at roughness amplitude $\epsilon = 0.02$. Other parameters are: $\beta = 0.07, \lambda = -0.6, \omega = 0.075, \Omega = 5, \omega_1 = 167, \omega_2 = 73$ and $f = 0.08$.

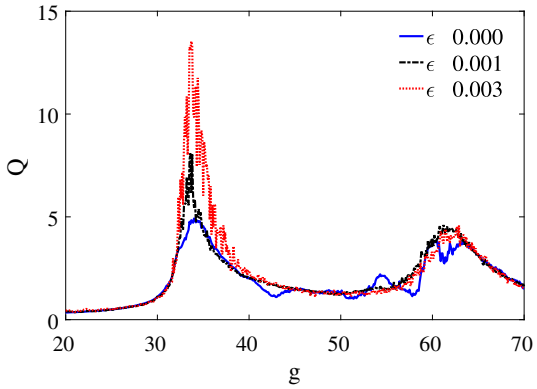

Figure 7. Dependence of the system's response amplitude (Q) on the amplitude of the fast signal (g) for three values of roughness amplitude, $\epsilon = 0, 0.002$, and 0.003. Other parameters are: $\mu = 4, \gamma = 0.01, \beta = 0.07, \lambda = 0.6, \omega = 0.08, \Omega = 5, \omega_1 = 167, \omega_2 = 73$ and $f = 0.1$.

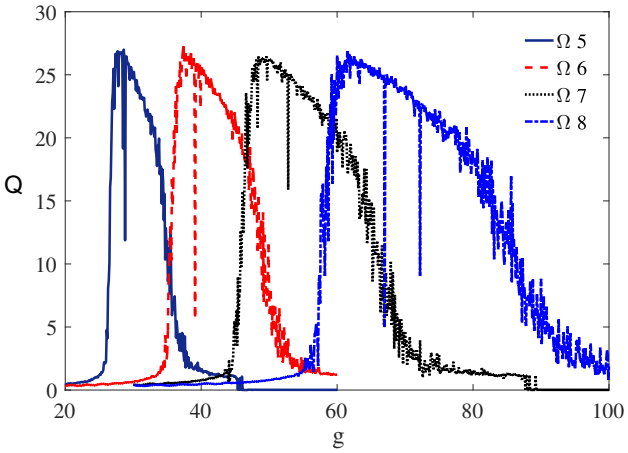

Figure 8. Dependence of Q on the amplitude of the fast signal for four values of the frequency of fast signal $\Omega = 5-8$. Other parameters are: $\mu = 4, \gamma = 0.01, \omega = 0.08, \beta = 0.07, \lambda = 0.6, \epsilon = 0.02, \omega_1 = 167$ and $\omega_2 = 73$.

negative values of γ one can obtain larger resonance peaks. On the contrary, small amplifications are achieved in the neighbourhood of $\gamma = 0.1$, corresponding to the value of γ used in other numerical simulations and providing insight into the contributions of other system parameters to the occurrence of VR. Finally, as γ approaches very large values, such that $\gamma \gg 0$, the system would not resonate. The emphasis here is that by truncating the higher-order nonlinear damping term, which is a requirement for the analytical solution given in eq. (24), the Q curve would appreciably differ in their peak values.

To examine the effect of higher-order nonlinearity on the observed resonance, the dependence of the system's response (Q) on the amplitude of the fast drive (g) for four values of the strength of higher-order nonlinear dissipation ($\gamma = 0.05, 0.07, 0.09$ and 0.1) for the system with smooth potential, $\epsilon = 0$ and other parameters; $\lambda = -0.6, \beta = 0.07, \Omega = 5, \omega_1 = 167$ and $\omega_2 = 73$ is presented in figure 6. The inset shows the same dependence $Q(g)$ for rugged potential landscape at roughness amplitude $\epsilon = 0.002$. At resonance, increasing the strength of the amplitude of higher-order nonlinearity significantly enhances the systems's response for both the smooth system and the rough system in similar manner within the set of parameters chosen.

To examine the effect of roughness on the system's response for fixed parameters $\mu = 4, \gamma = 0.01, \beta = 0.07, \lambda = -0.06, \omega = 0.08, \Omega = 25, \omega_1 = 167, \omega_2 = 73$ and $f = 0.1$, the response curve showing the dependence of Q (computed from eq. (29)) on g for four values of roughness amplitude, $\epsilon = 0, 0.002, 0.003$ and 0.004 is shown in figure 7. Undoubtedly, clear evidence of VR, a significant enhancement of resonance assisted by the roughness is observed as ϵ takes on nonzero values. The accompanying enhanced responses are distortions of the Q-curve arising from the potential roughness as shown in figure 7. Finally, in figure 8 depicting the dependence of Q on the amplitude of the fast signal for four frequencies of the fast signal $\Omega = 5-8$ with other parameters $\mu = 4, \gamma = 0.01, \omega = 0.08, \beta = 0.07, \lambda = -0.6$, and $\epsilon = 0.02, \omega_1 = 167$ and $\omega_2 = 73$ fixed, we find that increase in the frequency of fast signal increases the width of the response curve in the presence of potential roughness.

5. Conclusion

In this paper, we have examined VR of particles moving in a strongly nonlinear damped medium with a harmonically perturbed potential consisting of a background smooth triple-well potential superimposed by a fast oscillating spatial-dependent periodic function and subjected to LF and HF driving forces using theoretical and numerical methods. On the one hand, higher-order nonlinearity is found to contribute significantly to the occurrence of VR. Additionally, the higher-order nonlinearity produces similar effect on both the smooth potential and the rough potential. On the other hand, the spatial-dependent periodic function acting as potential roughness on the system's potential clearly created regimes of enhanced response amplitudes as well as distortion of the Q-curve smooth edge. Moreover, only the system's response to a smooth potential is remarkably affected within very small parameter values of the roughness amplitude but at such low values of the roughness, the relative magnitude of the maximum response $Q_{\max}$ remains almost independent of the roughness amplitude. Understanding the vibrational effects of higher-order nonlinear damping and potential ruggedness can shed light on applications to systems like single-mode Josephson-junction-based parametric amplifiers devices, wherein the effects of higher-order corrections, such as the presence of Kerr nonlinearities has significant impact on quantum efficiency, gain, phase matching of harmonic generation as well as output field squeezing [66–68].

Acknowledgements

U E Vincent is an alumnus of the Newton International Fellowships. He is supported by the Royal Society of London through their Newton International Fellowship Alumni Scheme.

References

[1] P S Landa and P V E McClintock, *J. Phys. A* **33**(**45**), L433 (2000)
[2] Y Ren, Y Pan, F Duan, F Chapeau-Blondeau and D Abbott, *Phys. Rev. E* **96**, 022141 (2017)
[3] H G Liu, X L Liu, J H Yang, M A F Sanjuán and G Cheng, *Nonlinear Dynam.* **89**(**4**), 2621 (2017)
[4] M I Dykman, D G Luchinsky, R Mannella, P V E McClintock, N D Stein and N G Stocks, *Il Nuovo Cimento D* **17**(**7–8**), 661 (1995)
[5] J Casado-Pascual, J Gómez-Ordónez and M Morillo, *Chaos* **15**(**2**), 26115 (2005)
[6] S Zambrano, J M Casado and M A F Sanjuán, *Phys. Lett. A* **366**, 428 (2007)
[7] A S Pikovsky and J Kurths, *Phys. Rev. Lett.* **78**(**5**), 775 (1997)
[8] S Rajasekar and M A F Sanjuán, Nonlinear resonances, *Springer series in synergetics* (Springer, Switzerland, 2016)
[9] S Rajamani, S Rajasekar and M A F Sanjuán, *Commun. Nonlin. Sci. Numer. Simulat.* **19**(**11**), 4003 (2014)
[10] R Jothimurugan, K Thamilmaran, S Rajasekar and M A F Sanjuán, *Nonlinear Dynam.* **83**(**4**),1803 (2016)
[11] M Gitterman, *J. Phys. A* **34**(**24**), L355 (2001)
[12] I I Blekhman and P S Landa, *Int. J. Non-Linear Mech.* **39**(**3**), 421 (2004)
[13] S Rajasekar, K Abirami and M A F Sanjuán, *Chaos* **21**(**3**), 033106 (2011)
[14] M Borromeo and F Marchesoni, *Phys. Rev. E* **73**, 016142 (2006)
[15] C Jeevarathinam, S Rajasekar and M A F Sanjuán, arXiv:1504.04163v1 [nlin.CD] (2015)
[16] S Jeyakumari, V Chinnathambi, S Rajasekar and M A F Sanjuán, *Int. J. Bifurc. Chaos* **21**(**1**), 275 (2011)
[17] Y Qin, J Wang, C Men, B Deng and X Wei, *Chaos* **21**(**2**), 023133 (2011)
[18] H Yu, J Wang, C Liu, B Deng and X Wei, *Chaos* **21**(**4**), 043101 (2011)
[19] X Wu, C Yao and J Shuai, *Sci. Rep.* **5**, 7684 (2015)
[20] Z Yang and L Ning, *Pramana – J. Phys.* **92**(**6**): 89 (2019)
[21] J P Baltanás, L López, I I Blechman, P S Landa, A Zaikin, J Kurths and M A F Sanjuán, *Phys. Rev. E* **67**, 066119 (2003)
[22] V N Chizhevsky, *Phys. Rev. E* **90**, 042924 (2014)
[23] P R Venkatesh and A Venkatesan, *Commun. Nonlin. Sci. Numer. Simulat.* **39**, 271 (2016)
[24] S Rajasekar, S Jeyakumari, V Chinnathambi and M A F Sanjuán, *J. Phys. A* **43**(**46**), 465101 (2010)
[25] J H Yang, M A F Sanjuán, W Xiang and H Zhu, *Pramana – J. Phys.* **81**(**6**), 943 (2013)
[26] B Deng, J Wang, X Wei, H Yu and H Li, *Phys. Rev. E* **89**, 062916 (2014)
[27] C Jeevarathinam, S Rajasekar and M A F Sanjuán, *Phys. Rev. E* **83**, 066205 (2011)
[28] J H Yang and X B Liu, *Phys. Scr.* **82**(**2**), 025006 (2010)
[29] J H Yang and X B Liu, *Chaos* **20**(**3**), 033124 (2010)
[30] J Yang and H Zhu, *Chaos* **22**(**1**), 013112 (2012)
[31] J H Yang, M A F Sanjuán, F Tian and H F Yang, *Int. J. Bifurc. Chaos* **25**(**02**), 1550023 (2015)
[32] T L M Djomo Mbong, M S Siewe and C Tchawoua, *Commun. Nonlin. Sci. Numer. Simulat.* **22**(**1**), 228 (2015)
[33] T O Roy-Layinde, J A Laoye, O O Popoola and U E Vincent, *Chaos* **26**, 093117 (2016)
[34] T O Roy-Layinde, J A Laoye, O O Popoola, U E Vincent and P V E McClintock, *Phys. Rev. E* **96**, 032209 (2017)
[35] U E Vincent, T O Roy-Layinde, O O Popoola, P O Adesina and P V E McClintock, *Phys. Rev. E* **98**, 062203 (2018)
[36] Z Chen and L Ning, *Pramana – J. Phys.* **90**: 49 (2018)

[37] S Jeyakumari, V Chinnathambi, S Rajasekar and M A F Sanjuán, *Chaos* **19**(**4**), 043128 (2009)
[38] S Jeyakumari, V Chinnathambi, S Rajasekar and M A F Sanjuán, *Phys. Rev. E* **80**, 046608 (2009)
[39] T L M D Mbong, M S Siewe and C Tchawoua, *Mech. Res. Commun.* **78**, 13 (2016)
[40] V N Chizhevsky, *Phys. Rev E* **89**, 062914 (2014)
[41] C Jeevarathinam, S Rajasekar and M A F Sanjuán, *Chaos* **23**(**1**), 013136 (2013)
[42] T Qin, T Xie, M Luo and K Deng, *Chin. J. Phys.* **55**(**2**), 546 (2017)
[43] P D'ancona and V Pierfelice, *J. Func. Anal.* **227**, 30 (2005)
[44] F Tantussi, D Vella, M Allegrini, F Fuso, L Romoli and C A Rashed, *Precis. Eng.* **41**, 32 (2015)
[45] C Ma, Y Duan, B Yu, J Sun and Q Tu, *J. Eng. Tribol.* **23**, 1307 (2017)
[46] R Zwanzig, *Proc. Natl. Acad. Sci.* **85**(**7**), 2029 (1988)
[47] S Banerjee, R Biswas, K Seki and B Bagchi, *J. Chem. Phys.* **141**, 124105 (2014)
[48] M Volk, L Milanesi, J P Waltho, C A Huntere and G S Beddardf, *Phys. Chem. Chem. Phys.* **17**(**2**), 762 (2015)
[49] L Milanesi, J P Waltho, C A Hunter, D J Shaw, G S Beddard, G D Reid, S Dev and M Volk, *Proc. Natl. Acad. Sci.* **109**(**48**), 19563 (2012)
[50] Y Zhou, H Zhu, W Zhang, X Zuo, Y Li and J Yang, *Adv. Mech. Eng.* **7**, 1 (2015)
[51] A Y Wang, J L Mo, X C Wang, M H Zhu and Z R Zhou, *Wear* **402–403**, 80 (2018)
[52] Y Li, Y Xu and J Kurths, *Phys. Rev. E* **96**, 052121 (2017)
[53] D Mondal, P Ghosh and D Ray, *J. Chem. Phys.* **130**(**7**), 074703 (2009)
[54] S Camargo and C Anteneodo, *Physica A* **495**, 114 (2018)
[55] Y Li, Y Xu, J Kurths and X Yue, *Chaos* **27**(**10**), 103102 (2017)
[56] Y Li, Y Xu, J Kurths and X Yue, *Phys. Rev. E* **94**, 042222 (2016)
[57] K Abirami, S Rajasekar and M A F Sanjuán, *Commun. Nonlin. Sci. Numer. Simulat.* **47**, 370 (2017)
[58] H G Enjieu Kadji, B R Nana Nbendjo, J B Chabi Orou and P K Talla, *Phys. Plasmas* **15**(**3**), 032308 (2008)
[59] M S Siewe, H Cao and M A F Sanjuán, *Chaos Solitons Fractals* **41**(**2**), 772 (2009)
[60] M S Siewe, M F M Kakmeni, C Tchawoua and P Woafo, *Nonlinear response, and homoclinic chaos of driven charge density in plasma*, Report 39090566 (International Atomic Energy Agency (IAEA), Abdus Salam International Centre for Theoretical Physics (Trieste, Italy, 2007))
[61] J Dawson, *Phys. Fluids* **7**(**7**), 981 (1964)
[62] H Okuda, *Phys. Fluids* **16**(**3**), 408 (1973)
[63] S Gitomer, R Jones, F Begay, A Ehler, J Kephart and R Kristal, *Phys. Fluids* **29**(**8**), 2679 (1986)
[64] F F Chen, *Phys. Plasmas* **2**(**6**), 2164 (1995)
[65] A Bystrov and V Gildenburg, *Plasma Phys. Rep.* **27**(**1**), 68 (2001)
[66] G Liu, T-C Chien, X Cao, O Lanes, E Alpern, D Pekker and M Hatridge, *Appl. Phys. Lett.* **111**(**20**), 202603 (2017)
[67] S Boutin, D M Toyli, A V Venkatramani, A W Eddins, I Siddiqi and A Blais, *Phys. Rev. Appl.* **8**, 054030 (2017)
[68] D L Weerawarne, X Gao, A L Gaeta and B Shim, *Phys. Rev. Lett.* **114**, 093901 (2015)